Chapter 2
Coupling Mechanism

Abstract An EMAT consists of a coil to induce dynamic electromagnetic fields at the surface region of a conductive material, and permanent magnets (or electromagnets) to provide a biasing magnetic field. An EMAT configuration depends on the modes of elastic waves to be excited and detected. Optimum design of an EMAT requires understanding the coupling mechanism of energy transfer between the electromagnetic and elastic fields. This is a long-running topic and many studies appeared (Thompson (1977, 1978, 1990); Kawashima (1976, 1985); Il'in and Kharitonov (1981); Wilbrand (1983, 1987); Ogi (1997); Ogi et al. (2003); Ribichini et al. (2012)). This chapter presents the comprehensive analysis on physical principles of EMATs.

Keywords Eddy current · Liftoff · Lorentz force · Magnetostriction · Piezomagnetic constants · Theoretical calculation

2.1 Background

Previous studies revealed that three mechanisms contribute to the coupling: (i) Lorentz force mechanism caused by the interaction between eddy currents and the static magnetic flux density, (ii) magnetization force mechanism between the oscillating magnetic field and the magnetization, and (iii) magnetostriction mechanism by the piezomagnetic effect. The Lorentz force mechanism arises in all conducting materials, while other two appear only in ferromagnetic materials. For nonmagnetic metals, therefore, the Lorentz force mechanism explains the transfer with an EMAT (Gaerttner et al. 1969). The coupling is rather complicated for ferromagnetic materials. Thompson (1978) studied the field dependence of the guided-wave amplitude in ferromagnetic thin plates and derived a theoretical model

M. Hirao and H. Ogi, *Electromagnetic Acoustic Transducers*,
Springer Series in Measurement Science and Technology,
DOI 10.1007/978-4-431-56036-4_2

to explain the results. Il'in and Kharitonov (1981) calculated the efficiency of detecting Rayleigh waves radiated by a meander-line coil in a ferromagnetic metal. Wilbrand (1983, 1987) discussed bulk-wave detection involving the three mechanisms. Following them, Ogi (1997) improved Wilbrand's model to explain the field dependence of the bulk-wave excitation and detection in a ferromagnetic metal. Ribichini et al. (2012) analyzed EMAT phenomenon in more practical cases with numerical simulations.

2.2 Generation Mechanism

2.2.1 Governing Equations

When an alternating current is applied to an EMAT's coil element placed near a ferromagnetic specimen, the electromagnetic fields occur and penetrate through the material. The fields inside the material interact with the biasing magnetic field, cause body forces, and generate elastic waves. Thus, the wave generation analysis takes three steps: (i) calculation of the electromagnetic fields inside the material (Sect. 2.2.2), (ii) calculation of the body forces caused by the interactions between the electromagnetic and elastic fields (Sects. 2.2.3–2.2.5), and (iii) calculation of the acoustic fields caused by the body forces.

The governing equations are Maxwell's equations (Ampere's law and Faraday's law of induction)

$$\mathrm{rot}\mathbf{H} = \frac{\partial \mathbf{D}}{\partial t} + \mathbf{J}, \tag{2.1}$$

$$\mathrm{rot}\mathbf{E} = -\frac{\partial \mathbf{B}}{\partial t}, \tag{2.2}$$

Ohm's law

$$\mathbf{J} = \eta \mathbf{E}, \tag{2.3}$$

the constitutive relation

$$\mathbf{B} = \mu_0 \mathbf{H} + \mathbf{M}, \tag{2.4}$$

and the equation of motion

$$\rho \frac{\partial^2 u_i}{\partial t^2} = \frac{\partial \sigma_{ij}}{\partial x_j} + f_i. \tag{2.5}$$

Summation convention is implied in Eq. (2.5). Here, **H** (A/m) denotes the magnetic field, **D** (C/m^2) the electric flux density, **J** (A/m^2) the current density, **E** (V/m) the electric field, **B** (T) the magnetic flux density, **M** (T) the magnetization, **f** (N/m^3) the body force per unit volume, and **u** (m) the elastic displacement. These are all vector quantities. σ_{ij} is a component of the stress tensor. μ_0 (= $4\pi \times 10^{-7}$ H/m) and η (S/m) are the free-space permeability and the electrical conductivity, respectively.

For a polycrystalline ferromagnetic material subjected to a homogeneous biasing magnetic field, the resulting magnetization shows anisotropy about the polarization direction. For example, when the biasing field is applied along the z-axis, the relationship between **M** and **H** takes the form

$$\mathbf{M} = [\chi]\mathbf{H} = \begin{bmatrix} \chi_{xx} & 0 & 0 \\ 0 & \chi_{xx} & 0 \\ 0 & 0 & \chi_{zz} \end{bmatrix} \mathbf{H}, \tag{2.6}$$

where $[\chi]$ denotes the magnetic susceptibility tensor. The **B**-**H** relationship can then be written as

$$\mathbf{B} = \mu_0 \begin{bmatrix} \bar{\mu}_{xx} & 0 & 0 \\ 0 & \bar{\mu}_{xx} & 0 \\ 0 & 0 & \bar{\mu}_{zz} \end{bmatrix} \mathbf{H}, \tag{2.7}$$

with the normalized permeability tensor $[\bar{\mu}]$, that is, $\bar{\mu}_{ij} = 1 + \chi_{ij}/\mu_0$.

2.2.2 *Dynamic Magnetic Fields in a Ferromagnetic Material*

For simplifying the analysis, we use several approximations. (i) The electromagnetic and elastodynamic fields are variables in the two-dimensional space of the x-z plane (see Fig. 2.1): The half-space of $z > 0$ is filled with a ferromagnetic metal with the isotropic permeability $\mu_0\bar{\mu}$, in which the x-y plane defines the interface with a vacuum. (ii) The magnetostriction causes no volume change (isovolume). This is true for a nontextured polycrystalline ferromagnetic material, because randomly oriented easy axes average out the anisotropic magnetostriction of individual magnetic domains (Chikazumi 1964). (iii) The displacement current $\partial\mathbf{D}/\partial t$ in Eq. (2.1) is neglected, because EMATs usually use frequencies of megahertz orders. (iv) All time-dependent quantities cause harmonic oscillation and involve the $e^{j\omega t}$ factor, which we omit in equations. Quantities with subscript 0 are time-independent and homogeneous.

We consider two basic coils as shown in Fig. 2.1: (a) unidirectionally aligned coils with n terns per unit length in the x-axis and (b) a meander-line coil with

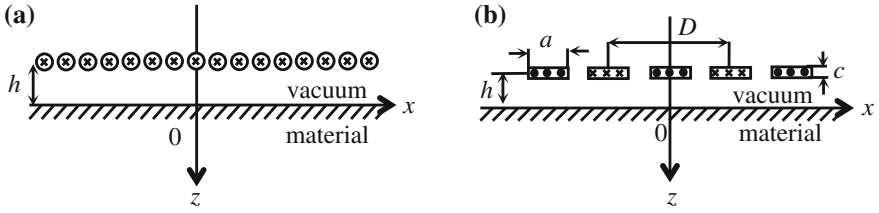

Fig. 2.1 Two-dimensional model of basic EMAT coils: **a** unidirectional coil and **b** meander-line coil

period D and width a. Current I flows in the coils. In this two-dimensional formulation, Eqs. (2.1)–(2.4) reduce to

$$\frac{\partial H_x}{\partial z} - \frac{\partial H_z}{\partial x} = J_y, \tag{2.8}$$

$$\frac{\partial E_y}{\partial z} = \mu_0 \bar{\mu} \frac{\partial H_x}{\partial t}, \tag{2.9}$$

$$\frac{\partial E_y}{\partial x} = -\mu_0 \bar{\mu} \frac{\partial H_z}{\partial t}, \tag{2.10}$$

$$J_y = \eta E_y. \tag{2.11}$$

Comparison between the x derivative of Eq. (2.9) and the z derivative of Eq. (2.10) leads to

$$\frac{\partial H_x}{\partial x} = -\frac{\partial H_z}{\partial z}. \tag{2.12}$$

Differentiating Eq. (2.8) with respect to z and using Eqs. (2.9), (2.11), and (2.12), we have

$$\left(\frac{\partial^2}{\partial x^2} + \frac{\partial^2}{\partial z^2}\right) H_x - j\omega\eta\mu_0\bar{\mu} H_x = 0. \tag{2.13}$$

In a vacuum, H_x satisfies Laplace equation

$$\left(\frac{\partial^2}{\partial x^2} + \frac{\partial^2}{\partial z^2}\right) H_x^V = 0. \tag{2.14}$$

For the unidirectional coil (Fig. 2.1a), a current element at x, $nI\mathrm{d}x$, provides the tangential magnetic field at the origin, which is obtained by superimposing the fields caused by the original element $nI\mathrm{d}x$ and its reflection image $nI\mathrm{d}x(\bar{\mu} - 1)/(\bar{\mu} + 1)$ (Hammond and Sykluski 1994)

$$\mathrm{d}H_x^V = \frac{nI\mathrm{d}x}{2\pi(x^2+h^2)} \cdot \frac{2h}{\bar{\mu}+1}.$$

Thus, the total tangential field at $z = 0$ caused by the sheet currents is given by

$$H_x^V = 2\int_0^\infty \mathrm{d}H_x^V = 2 \times \frac{nI}{\pi(\bar{\mu}+1)} \int_0^\infty \frac{h}{x^2+h^2}\mathrm{d}x = \frac{nI}{\bar{\mu}+1}, \tag{2.15}$$

using a formula

$$\int_0^\infty \frac{h}{x^2+h^2}\mathrm{d}x = \frac{\pi}{2}.$$

The magnetic field in the material, H_x^M, must satisfy Eq. (2.13) and the electromagnetic boundary condition at the interface

$$H_x^V(x,0) = H_x^M(x,0) = \frac{nI}{\bar{\mu}+1}. \tag{2.16}$$

Because $\partial/\partial x = 0$ for all quantities, Eq. (2.13) can be written as

$$\frac{\partial^2 H_x^M}{\partial z^2} - q^2 H_x^M = 0, \tag{2.17}$$

where

$$q \equiv -\frac{1}{\delta}(1+j), \tag{2.18}$$

$$\delta = \sqrt{\frac{2}{\omega\eta\mu_0\bar{\mu}}}. \tag{2.19}$$

The solution of Eq. (2.17), which does not diverge at $z \to \infty$ and satisfies the boundary condition of Eq. (2.16), is

$$H_x^M = \frac{nI}{\bar{\mu}+1}e^{qz} = \frac{nI}{\bar{\mu}+1}e^{-\frac{z}{\delta}}e^{-j\frac{z}{\delta}}. \tag{2.20}$$

The magnetic field decays exponentially in the z direction depending on a factor $1/\delta$. The penetration depth is represented by δ and is called the *electromagnetic skin depth*. For copper at 1 MHz, $\delta \approx 0.07$ mm. For steels, $\delta \approx 0.01$ mm. Thus, δ is much smaller than the ultrasonic wavelength used in EMAT measurements, and it can be assumed that the electromagnetic fields occur only at the material surfaces.

Concerning the meander-line coil (Fig. 2.1b), the calculation of the fields inside the material is explained in detail in Thompson's monograph (Thompson 1990). The current per unit length along the x-axis of the meander-line coil is given by

$$\frac{I}{a}s(x), \quad \text{where} \quad s(x) = \begin{cases} 1, & -a/2 < x < a/2 \\ 0, & -(D-a)/2 < x < -a/2 \text{ or } a/2 < x < (D-a)/2 \\ -1, & -D/2 < x < -(D-a)/2 \text{ or } (D-a)/2 < x < D/2 \end{cases}. \tag{2.21}$$

$s(x)$ can be expressed by a Fourier series,

$$s(x) = \sum_m A_m \cos\, k_m x, \tag{2.22}$$

where

$$A_m = \frac{4}{(2m+1)\pi} \sin\left\{\frac{a}{D}(2m+1)\pi\right\}, \tag{2.23}$$

$$k_m = \frac{2\pi}{D}(2m+1). \tag{2.24}$$

The integrated form of Eq. (2.1) gives the relationship that the contour integral of the magnetic field along the closed curve surrounding the meander-line current equals the total current passing through the cross section. This gives the magnetic field beneath the meander-line coil:

$$H_x^V(x, -h) = \sum_m \frac{I}{2a} A_m \cos\, k_m x. \tag{2.25}$$

Supposing $\partial^2/\partial x^2 = -k_m^2$, the solution of Eq. (2.14) that satisfies the boundary condition of Eq. (2.25) and does not diverge at $z \to \infty$ becomes

$$H_x^V = \sum_m \frac{I}{2a} A_m e^{-k_m h} e^{-k_m z} \cos\, k_m x. \tag{2.26}$$

Equation (2.12) leads to

$$H_z^V = -\sum_m \frac{I}{2a} A_m e^{-k_m h} e^{-k_m z} \sin\, k_m x. \tag{2.27}$$

Solutions (2.26) and (2.27) express the magnetic fields below the meander-line coil in vacuum. They involve the factor $e^{-k_m h}$, which rapidly decays with increasing m. For simplicity, only the first term (m = 0) is considered:

$$\begin{cases} H_x^V = \dfrac{I}{2a} A_0 e^{-k_0 h} e^{-k_0 z} \cos\, k_0 x, \\ H_z^V = -\dfrac{I}{2a} A_0 e^{-k_0 h} e^{-k_0 z} \sin\, k_0 x. \end{cases} \tag{2.28}$$

The image method is then applied to calculate the magnetic field with the presence of the half-space conductor:

$$\begin{cases} H_x^M = IaA_0 e^{-k_0 h} e^{qz} \cos\, k_0 x, \\ H_z^M = k_0 \delta \sqrt{2} IaA_0 e^{-j\frac{\pi}{4}} e^{-k_0 h} e^{qz} \sin\, k_0 x. \end{cases} \tag{2.29}$$

where $q^2 = k_0^2 + 2j/\delta^2$ ($\mathrm{Re}(q) < 0$). We used a reasonable approximation that $k\delta \ll 1$ and then $\left|H_x^M\right| \gg \left|H_z^M\right|$. The presence of the gap h between the coil and material surface, called *liftoff*, exponentially decreases the magnitude of the electromagnetic fields in the material.

The magnetic fields induced by EMAT coils in the material take the form

$$\begin{cases} H_x^M = f(x) e^{qz} \\ H_z^M = g(x) e^{qz} \end{cases}, \tag{2.30}$$

where f and g are functions of only x. Because the variable changes in the z-axis are much larger than in the x-axis ($k_0\delta \ll 1$), the following relation usually holds

$$\left|\frac{\partial H_x^M}{\partial z}\right| \gg \left|\frac{\partial H_x^M}{\partial x}\right| \approx \left|\frac{\partial H_z^M}{\partial z}\right| \gg \left|\frac{\partial H_z^M}{\partial x}\right|. \tag{2.31}$$

2.2.3 Lorentz Force

The Lorentz force mechanism was studied by many researchers (Gaerttne et al. 1969; Beissner 1976; Kawashima 1976; Maxfield and Fortunko 1983; Thompson 1973, 1990). We summarize their studies here.

When an electric field $\mathbf{E}$ is applied to a conducting material, the Coulomb force $-e\mathbf{E}$ occurs on individual electrons. In the presence of the biasing magnetic field $\mathbf{B}_0$, the Lorentz force $e\mathbf{v}_e \times \mathbf{B}_0$ appears. $\mathbf{v}_e$ denotes the mean electron velocity. Thus, the equation of motion for an electron is

$$m\dot{\mathbf{v}}_e = -e(\mathbf{E} + \mathbf{v}_e \times \mathbf{B}_0) - \frac{m\mathbf{v}_e}{\tau}. \tag{2.32}$$

Here, m denotes the electron mass and e denotes the electron charge. τ denotes the mean time of the electron-ion collision and is of the order of 10^{-14} s for common metals at room temperature. Supposing harmonic oscillation of the electric field with the angular frequency ω and $\omega\tau \ll 1$, Eq. (2.32) reduces to

$$n_e \frac{m\mathbf{v}_e}{\tau} = -n_e e(\mathbf{E} + \mathbf{v}_e \times \mathbf{B}_0), \tag{2.33}$$

where n_e is the electron density. This momentum is transferred to the ions via the collisions. Thus, the body forces applied to the ions are approximated as

$$\mathbf{f} = NZ_e(\mathbf{E} + \dot{\mathbf{u}} \times \mathbf{B}_0) + n_e \frac{m\mathbf{v}_e}{\tau}, \tag{2.34}$$

where N denotes the ion density, Z_e the ion charge, and $\mathbf{u}$ the ion displacement. Because $n_e e = NZ_e$ and $\mathbf{v}_e \gg \dot{\mathbf{u}}$, the force per unit volume on ions reduces to

$$\mathbf{f} = -n_e e\mathbf{v}_e \times \mathbf{B}_0 = \mathbf{J}_e \times \mathbf{B}_0 \equiv \mathbf{f}^{(L)}. \tag{2.35}$$

$\mathbf{J}_e = -n_e e\mathbf{v}_e$ is the electron eddy current density. The Lorentz force in Eq. (2.35) can cause an acoustic vibration.

From Eq. (2.8), we have

$$J_e = \frac{\partial H_x^M}{\partial z} - \frac{\partial H_z^M}{\partial x}. \tag{2.36}$$

According to Eq. (2.31), the second term in the right-hand side is negligible compared with the first term. Then, the Lorentz forces are

$$\begin{cases} f_x^{(L)} = B_{0z} \dfrac{\partial H_x^M}{\partial z}, \\ f_z^{(L)} = -B_{0x} \dfrac{\partial H_x^M}{\partial z}. \end{cases} \tag{2.37}$$

When we consider the contribution of the dynamic magnetic field $\mathbf{B}$ caused by the EMAT coil as well as the static field, the Lorentz forces are expressed by

$$\begin{cases} f_x^{(L)} = (B_{0z} + \mu_0 \bar{\mu} H_z^M) \dfrac{\partial H_x^M}{\partial z}, \\ f_z^{(L)} = -(B_{0x} + \mu_0 \bar{\mu} H_x^M) \dfrac{\partial H_x^M}{\partial z}. \end{cases} \tag{2.38}$$

Equation (2.7) is used. Thus, the Lorentz forces caused by the static field (first terms of the right-hand sides) are proportional to the driving current I and vibrate with the same frequency ω as the driving current. Whereas those caused by the dynamic field (second terms) are proportional to I^2 and possess the doubled frequency component of 2ω. Because the magnitude of the static field is usually much larger than that of the dynamic field, we can neglect the second terms. However, when a large driving current is in use, the second terms exceed the first terms to

give rise to the double-frequency ultrasound. Such an excitation requires no static field and makes the EMAT compact as will be shown in Sect. 18.4.2.

2.2.4 Magnetization Force

The force acting in the volume and on the surface of a magnetic material because of the presence of the magnetization **M** are summed up to give (Brown 1966; Moon 1984)

$$\mathbf{F} = \int_V \mathbf{M} \cdot \nabla \mathbf{H} \, \mathrm{d}V + \frac{1}{2}\mu_0 \int_S \mathbf{n} M_n^2 \mathrm{d}S. \tag{2.39}$$

n is a unit vector normal to the material surface and M_n the normal component of the magnetization at the surface. The second term in Eq. (2.39) appears because of a steep change of the electromagnetic fields at the surface and disappears inside the material. The integrand in the first term of Eq. (2.39) consists of gradients of dynamic magnetic field, involving some components of Eq. (2.35). In this book, we remain the definition for the Lorentz force mechanism in Eq. (2.35) and regard the body force per unit volume

$$\mathbf{f}^{(M)} = (\nabla \mathbf{H}) \cdot \mathbf{M}_0, \tag{2.40}$$

as the magnetization force. When the biasing magnetic field is applied, Eq. (2.40) becomes

$$\begin{cases} f_x^{(M)} = M_{0x} \dfrac{\partial H_x^M}{\partial x} + M_{0z} \dfrac{\partial H_z^M}{\partial x}, \\ f_z^{(M)} = M_{0x} \dfrac{\partial H_x^M}{\partial z} + M_{0z} \dfrac{\partial H_z^M}{\partial z}. \end{cases} \tag{2.41}$$

The second terms are negligible because of $\left|H_x^M\right| \gg \left|H_z^M\right|$. Combining with the Lorentz forces in Eq. (2.37) and using Eq. (2.4), we obtain

$$\begin{cases} f_x^{(M)} + f_x^{(L)} = B_{0z} \dfrac{\partial H_x^M}{\partial z} + M_{0x} \dfrac{\partial H_x^M}{\partial x}, \\ f_z^{(M)} + f_z^{(L)} = (M_{0x} - B_{0x}) \dfrac{\partial H_x^M}{\partial z} = -\mu_0 H_{0x} \dfrac{\partial H_x^M}{\partial z}. \end{cases} \tag{2.42}$$

The biasing magnetic field in EMAT phenomena is normally less than a few Tesla and $|\mu_0 \mathbf{H}_0| \ll |\mathbf{M}_0|$. It is important to note that, in the case of a tangential biasing magnetic field ($H_{0z} = 0$), $f_z^{(L)}$ and $f_z^{(M)}$ act in opposite directions and the magnetization force cancels a major part of the Lorentz force in the z direction. Thus, the

Lorentz and magnetization forces are ineffective in generating longitudinal-mode waves in ferromagnetic materials.

The magnetizaiton force defined in Eq. (2.40) applies in most cases, but it fails to explain the wave generation in some particular cases, for which the total magnetic forces in Eq. (2.39) have to be considered (Seher and Nagy 2016).

2.2.5 *Magnetostriction Force*

When an external magnetic field is applied to a ferromagnetic material, a dimensional change arises depending on the magnitude and direction of the field. The normalized dimensional change is called *magnetostriction*. It occurs because, in iron for instance, the external magnetic field affects the 3*d* subshell and changes the shape and size of the 3*d*-electron orbits to minimize energy in the presence of the field. This can be intuitively understood by considering a dimensional change in a magnetic domain caused by the rotation of magnets connected by elastic springs (Fig. 2.2). The magnets simulate atomic spins. There is an elastic strain to make a balance between the spring and magnetic forces in equilibrium even without an external field, which is the spontaneous magnetostriction and is equivalent to an eigenstrain in individual magnetic domains. In iron, a positive spontaneous magnetization exists in domain's magnetization directions oriented to easy axes <100>.

In polycrystalline materials, the magnetostriction response to the external field is more complicated. In polycrystalline iron, the dimensional change occurs in two steps. First, the domains, whose magnetizations are oriented near along the external field, expand in volume, causing a positive dimensional change (elongation) along the field because of the positive spontaneous magnetostriction (Fig. 2.3b). After this domain's rearrangement, the magnetization rotates about the easy axis within the domain, which reduces the dimension due to the rotation of the spins. Thus, the magnetostriction ε^{M} along the applied field is a function of the external field H and

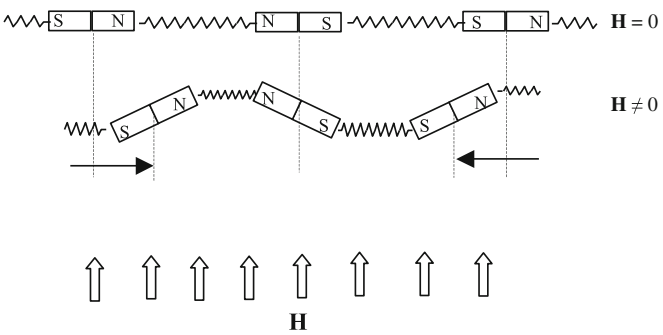

Fig. 2.2 Intuitive understanding of magnetostriction in a magnetic domain. Dimensional change caused by the external field on magnets connected to each other by elastic springs corresponds to magnetostriction

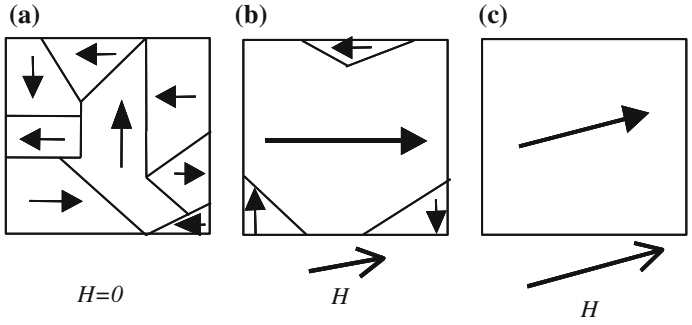

Fig. 2.3 Evolution of domains and rotation of magnetization with the increase of the external field in a polycrystalline (or multi-domain) material. **a** Randomly oriented domains at $H = 0$. **b** Volume increase in the domain oriented nearly parallel to the field. **c** Rotation of the magnetization to the field direction

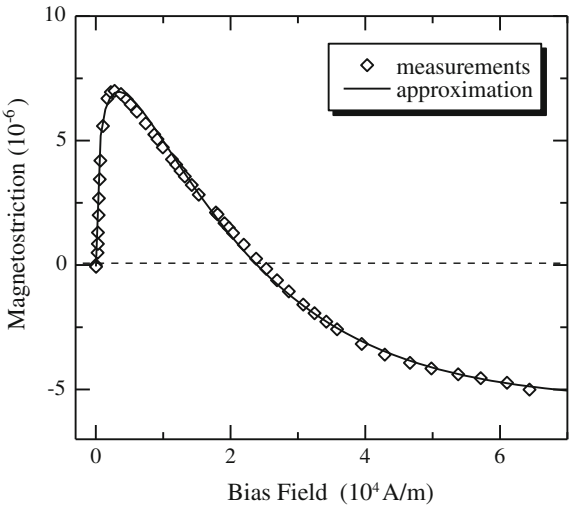

Fig. 2.4 Measured (*open symbols*) and approximated (*solid line*) magnetostriction curve for a low-carbon steel

then the ε-H curve, or the magnetostriction curve, shows a maximum. Figure 2.4 exemplifies the measured magnetization curve for a low-carbon steel. The magnitude of maximum magnetostriction is of the order of 10^{-6} for steels and 10^{-5} for nickel.

Coupling between the elastic and magnetic fields for such a ferromagnetic (or piezomagnetic) material can be assumed to take a similar form as that for a piezoelectric material:

$$S_I = d_{Ij}^{(MS)} H_j + s_{IJ}^H \sigma_J. \quad (I, J = 1, 2, \ldots, 6;\ j = x, y, z) \tag{2.43}$$

Here, S_I is a component of the engineering strain, s_{IJ}^H a component of the compliance matrix at a constant field, and σ_J the stress component in contracted notation (Auld 1973). $d_{Ij}^{(MS)}$ can be written as

$$d_{Ij}^{(MS)} = \left(\frac{\partial S_I}{\partial H_j}\right)_{|\sigma}, \tag{2.44}$$

which indicate the piezomagnetic strain coefficients. When we apply a magnetic field to a ferromagnetic material at the stress-free state, the strain $S_I = d_{Ij}^{(MS)} H_j$ will appear. The same strain field occurs with the stress field $\sigma_K = c_{KI}^H S_I$ without the magnetic field, where c_{KI}^H is the elastic-stiffness coefficient at a constant field. The equivalent stress to cause the magnetostriction is $\sigma_K = c_{KI}^H d_{Ij}^{(MS)} H_j$. If the applied magnetic field changes quickly or vibrates with a high frequency, the strain will fail to respond simultaneously with the field and the stress field $-\sigma_K$ will occur inside the material, which is the magnetostriction stress. We can thus define the magnetostriction stress as

$$\sigma_I^{(MS)} = -c_{IJ}^H d_{Jj}^{(MS)} H_j = -e_{Ij}^{(MS)} H_j, \tag{2.45}$$

with the converse piezomagnetic stress coefficients

$$e_{Ij}^{(MS)} = c_{IJ}^H d_{Jj}^{(MS)} = -\left(\frac{\partial \sigma_I^{(MS)}}{\partial H_j}\right)_{|S}. \tag{2.46}$$

The constitutive equation among the stress, strain, and field is then given by

$$\sigma_I = -e_{Ij}^{(MS)} H_j + c_{IJ}^H S_J, \tag{2.47}$$

Equation (2.47) is similar to that of the piezoelectric stress equation. The body forces caused by the magnetostriction stress are

$$\begin{cases} f_x^{(MS)} = \dfrac{\partial \sigma_1^{(MS)}}{\partial x} + \dfrac{\partial \sigma_6^{(MS)}}{\partial y} + \dfrac{\partial \sigma_5^{(MS)}}{\partial z}, \\ f_y^{(MS)} = \dfrac{\partial \sigma_6^{(MS)}}{\partial x} + \dfrac{\partial \sigma_2^{(MS)}}{\partial y} + \dfrac{\partial \sigma_4^{(MS)}}{\partial z}, \\ f_z^{(MS)} = \dfrac{\partial \sigma_5^{(MS)}}{\partial x} + \dfrac{\partial \sigma_4^{(MS)}}{\partial y} + \dfrac{\partial \sigma_3^{(MS)}}{\partial z}. \end{cases} \tag{2.48}$$

The acoustic fields generated by the magnetostriction forces can be calculated using Eqs. (2.5) and (2.48) with boundary conditions when the piezomagnetic coefficients $\mathbf{d}^{(MS)}$ and $\mathbf{e}^{(MS)}$ are known. They depend highly on the magnitude and direction of the applied field, but they are estimated from the magnetostriction curve as exemplified in Fig. 2.4. Following are the examples for calculating the piezomagnetic coefficients.

(a) Bias field normal to the surface ($\mathbf{H}_0 = (0, 0, H_{0z})$)

When a homogenous static magnetic field H_{0z} is applied in the z direction (normal to the specimen surface) in a ferromagnetic material in the stress-free state, the longitudinal magnetostriction $\varepsilon(H_{0z})$ appears along the field. The magnetostriction perpendicular to the field will be $-\varepsilon(H_{0z})/2$ because of the isovolume dimensional change. Thus, the time-independent strain field $\mathbf{S}^0$ caused by the applied field is

$$S_3^0 = \varepsilon(H_{0z}), \quad S_1^0 = S_2^0 = -\frac{1}{2}\varepsilon(H_{0z}), \quad S_4^0 = S_5^0 = S_6^0 = 0. \tag{2.49}$$

The dynamic field applied in the z direction, H_z, disturbs the strain field to cause the dynamic strain $\mathbf{S}$. When the dynamic field is much smaller in magnitude than the static field, we can approximate as

$$\begin{aligned} &S_3 = \left(\frac{\partial S_3}{\partial H_z}\right) H_z, \quad S_1 = S_2 = -\frac{1}{2}\left(\frac{\partial S_3}{\partial H_z}\right) H_z, \\ &S_4 = S_5 = S_6 = 0. \end{aligned} \tag{2.50}$$

The piezomagnetic strain coefficients related to the field in the z direction are therefore given by

$$\begin{cases} d_{3z}^{(MS)} = \left(\dfrac{\partial S_3}{\partial H_z}\right)_{|\sigma} \equiv \gamma, \quad d_{1z}^{(MS)} = d_{2z}^{(MS)} = -\frac{1}{2}\gamma, \\ d_{4z}^{(MS)} = d_{5z}^{(MS)} = d_{6z}^{(MS)} = 0, \end{cases} \tag{2.51}$$

which indicates that the shearing deformation is not caused by H_z. γ denotes the slope of the magnetostriction curve and is measurable.

Components of the coefficients related to the x direction dynamic field can be calculated as follows. When the dynamic field H_x is added, the total field occurs in the direction inclined by θ about the z-axis and the principal strains arise in the directions parallel and normal to the total field. Thus, in the coordinate system where the z'-axis is along the total field (Fig. 2.5), the strains can be expressed as

$$S_3' = \varepsilon(H_t) \equiv \varepsilon_t, \quad S_1' = S_2' = -\frac{1}{2}\varepsilon(H_t) = -\frac{1}{2}\varepsilon_t, \tag{2.52}$$

where ε_t denotes the magnetostriction along the total field $\mathbf{H}_t$. Note that no shearing deformation occurs in the x'-y'-z' coordinate system. The strain field in the original coordinate system takes the form

$$\begin{cases} S_1 = S_1' \cos^2\theta + S_3' \sin^2\theta, \\ S_2 = S_2', \\ S_3 = S_3' \cos^2\theta + S_1' \sin^2\theta, \\ S_5 = (S_3' - S_1') \sin 2\theta = \frac{3}{2}\varepsilon_t \sin 2\theta. \end{cases} \tag{2.53}$$

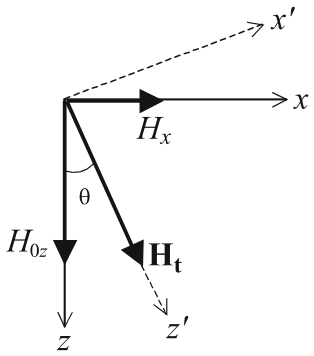

Fig. 2.5 Rotation of the total field about the static field direction

It is clear that $d_{4x}^{(MS)} = d_{6x}^{(MS)} = 0$ because S_4 and S_6 equal zero. Then, we have

$$\begin{cases} d_{1x}^{(MS)} = \left(\dfrac{\partial S_1}{\partial H_x}\right)_{|\sigma} = \dfrac{\partial}{\partial H_x}(S_1' \cos^2\theta + S_3' \sin^2\theta) \\ \qquad = \dfrac{3\varepsilon_t}{H_{0z}} \cos^3\theta \sin\theta + \gamma \sin\theta\left(-\dfrac{1}{2}\cos^2\theta + \sin^2\theta\right), \\ d_{2x}^{(MS)} = -\dfrac{1}{2}\gamma \sin\theta, \\ d_{3x}^{(MS)} = -\dfrac{3\varepsilon_t}{H_{0z}} \cos^3\theta \sin\theta + \gamma \sin\theta\left(-\dfrac{1}{2}\sin^2\theta + \cos^2\theta\right), \\ d_{5x}^{(MS)} = \dfrac{3\gamma}{2}\sin 2\theta \sin\theta + \dfrac{3\varepsilon_t}{H_{0z}} \cos^2\theta \cos 2\theta. \end{cases} \tag{2.54}$$

Analogous calculation results in the coefficients relating to H_y:

$$\begin{cases} d_{1y}^{(MS)} = d_{2x}^{(MS)},\ d_{2y}^{(MS)} = d_{1x}^{(MS)},\ d_{3y}^{(MS)} = d_{3x}^{(MS)},\ d_{4y}^{(MS)} = d_{5x}^{(MS)}, \\ d_{5y}^{(MS)} = d_{6y}^{(MS)} = 0. \end{cases} \tag{2.55}$$

Thus, the matrix $\mathbf{d}^{(MS)}$ takes the following form for the normal bias field,

$$\left[d_{lj}^{(MS)}\right] = \begin{bmatrix} d_{1x} & d_{2x} & d_{1z} \\ d_{2x} & d_{1x} & d_{1z} \\ d_{3x} & d_{3x} & d_{3z} \\ 0 & d_{5x} & 0 \\ d_{5x} & 0 & 0 \\ 0 & 0 & 0 \end{bmatrix}. \tag{2.56}$$

EMATs normally use a static magnetic field much larger than the dynamic fields, that is, $H_{0z} \gg H_x$ and H_z. Such a high-field approximation reduces Eq. (2.56) to

$$\left[d_{lj}^{(MS)}\right] = \begin{bmatrix} 0 & 0 & -\frac{\gamma}{2} \\ 0 & 0 & -\frac{\gamma}{2} \\ 0 & 0 & \gamma \\ 0 & \frac{3\varepsilon_t}{H_{0z}} & 0 \\ \frac{3\varepsilon_t}{H_{0z}} & 0 & 0 \\ 0 & 0 & 0 \end{bmatrix}. \tag{2.57}$$

Equation (2.57) is comparable with the piezoelectric strain coefficients of crystals, which belong to a hexagonal 6*mm* point group.

Equations (2.48) and (2.57) are combined to derive the two-dimensional magnetostriction forces as

$$f_x^{(MS)} = -\frac{3c_{55}\varepsilon_t}{H_{0z}}\frac{\partial H_x}{\partial z} + \frac{\gamma}{2}(c_{11} - c_{12})\frac{\partial H_z}{\partial x}, \tag{2.58}$$

$$f_z^{(MS)} = -\frac{3c_{55}\varepsilon_t}{H_{0z}}\frac{\partial H_x}{\partial x} - \gamma(c_{11} - c_{12})\frac{\partial H_z}{\partial z}. \tag{2.59}$$

Equation (2.31) allows us to neglect the second term on the right-hand side of Eq. (2.58) and to predict $\left|f_x^{(MS)}\right| \gg \left|f_z^{(MS)}\right|$, indicating that the shear wave polarized in the x direction can be generated more efficiently than the longitudinal wave with the magnetostriction forces.

It is important to note that the stress-free condition at the surface needs the apparent traction force, which markedly cancels the magnetostriction force $f_x^{(MS)}$ (Ribichini et al. 2012). The contribution of the magnetostriction mechanism to the wave generation is comparable with that of the Lorentz force mechanism in lower magnetic field region ($\lesssim$1000 A/m). However, it becomes minor at higher field (Ogi 2012).

For example, consider the shear plane wave generation by the sheet current as shown in Fig. 2.1a and a homogenous normal magnetic field B_{0z}. The wave equation takes the form

$$\rho\frac{\partial^2 u_x}{\partial t^2} = \frac{\partial \sigma_5}{\partial z} + B_{0z}\frac{\partial H_x^M}{\partial z}, \tag{2.60}$$

where

$$\sigma_5 = G\frac{\partial u_x}{\partial z} - e_{5x}^{(MS)}H_x^M. \tag{2.61}$$

G denotes the shear modulus, and H_x^M is given by Eq. (2.20). Assuming the harmonic vibration with ω, we have

$$\frac{\partial^2 u_x}{\partial z^2} + K^2 u_x = \frac{Pq}{G}\left(e_{5x}^{(MS)} - B_{0z}\right)e^{qz}e^{j\omega t}. \tag{2.62}$$

Here, $K \equiv \omega\sqrt{\rho/G}$ and $P \equiv nI/(1+\bar{\mu})$. The general solution takes the form $u_x = (A^* e^{-jKz} + B^* e^{qz})e^{j\omega t}$, where A^* and B^* denote complex coefficients: The first term represents the homogeneous solution, allowing long-distance propagation, and is important for EMAT applications. The second term indicates a particular solution, which decays rapidly with propagation. Substituting this form into Eq. (2.62) yields

$$B^* = \frac{P}{G}\left(e_{5x}^{(MS)} - B_{0z}\right)\frac{q}{q^2 + K^2}. \tag{2.63}$$

From the boundary condition ($\sigma_5 = 0$ at $z = 0$) and Eq. (2.63), we have

$$A^* \approx \frac{P}{KG}\left(\frac{e_{5x}^{(MS)}}{2}(K\delta)^2 + jB_{0z}\right), \tag{2.64}$$

with $|K\delta| \ll 1$. The first and second terms show contributions of the magnetostriction and Lorentz-force mechanisms, respectively. Their ratio, $(K\delta)^2 e_{5x}^{(MS)}/2B_{0z}$, then indicates dominant mechanism. Assuming $e_{5x}^{(MS)} = 3G\varepsilon_t/H_{0z}$ with $G = 80$ GPa and $\varepsilon_t = 2 \times 10^{-6}$, frequency of 5 MHz, conductivity of 5×10^6 S/m, $B_{0z} = 0.3$ T, and $\bar{\mu} = 1000$, this ratio becomes about unity when $H_{0z} = 1000$ A/m. It becomes less than 0.1 for $H_{0z} = 10{,}000$ A/m, indicating the dominant contribution of the Lorentz force mechanism at higher magnetic field.

(b) Bias field parallel to the surface in the y-axis ($\mathbf{H}_0 = (0, H_{0y}, 0)$)

A similar approach to the above yields an expression for the piezomagnetic coefficients for a bias field in the y direction;

$$\left[d_{Ij}^{(MS)}\right] = \begin{bmatrix} d_{1x} & d_{1y} & d_{3x} \\ d_{2x} & d_{2y} & d_{2x} \\ d_{3x} & d_{1y} & d_{1x} \\ 0 & 0 & d_{6x} \\ 0 & 0 & 0 \\ d_{6x} & 0 & 0 \end{bmatrix}. \tag{2.65}$$

For example,

$$d_{6x}^{(MS)} = \frac{3\gamma}{2}\sin 2\theta \sin\theta + \frac{3\varepsilon_t}{H_{0y}}\cos^2\theta \cos 2\theta. \tag{2.66}$$

At high fields ($H_{0y} \gg H_x$, H_z), Eq. (2.65) reduces to

$$\left[d_{Ij}^{(MS)}\right] = \begin{bmatrix} 0 & -\frac{\gamma}{2} & 0 \\ 0 & \gamma & 0 \\ 0 & -\frac{\gamma}{2} & 0 \\ 0 & 0 & \frac{3\varepsilon_t}{H_{0y}} \\ 0 & 0 & 0 \\ \frac{3\varepsilon_t}{H_{0y}} & 0 & 0 \end{bmatrix} \tag{2.67}$$

The nonzero body force occurs only in the y direction in this case:

$$f_y^{(MS)} = \frac{\partial \sigma_6^{(MS)}}{\partial x} + \frac{\partial \sigma_4^{(MS)}}{\partial z} = -\frac{3c_{66}\varepsilon_t}{H_{0y}}\frac{\partial H_x}{\partial x} - \frac{3c_{44}\varepsilon_t}{H_{0y}}\frac{\partial H_z}{\partial z}, \tag{2.68}$$

where we neglected the terms proportional to $\partial H_z/\partial x$. The first term in the right-hand side of Eq. (2.68) can generate the surface shear waves or plate shear waves propagating in the x direction with the y polarization. The second term generates the bulk shear wave propagating in the thickness direction with the y polarization.

2.3 Receiving Mechanisms

A dynamic deformation caused by an acoustic wave creates dynamic electromagnetic fields in a conductive material exposed to a steady magnetic field. The dynamic fields pass the material/vacuum boundary and can be detected by an EMAT coil. The analysis of EMAT's receiving mechanism then includes three factors: (i) the electromagnetic fields within the material caused by elastic waves, (ii) moving boundary at the material surface, through which the fields pass into a vacuum, and (iii) the electromagnetic fields in vacuum, where the EMAT coil is located.

The dynamic electric field induced by the deformation in a conducting material takes the form

$$\frac{\partial \mathbf{u}}{\partial t} \times \mathbf{B}_0. \tag{2.69}$$

This is the reversed Lorentz force mechanism. The induced current density in the material can be of the form

$$\mathbf{J} = \eta\left(\mathbf{E} + \frac{\partial \mathbf{u}}{\partial t} \times \mathbf{B}_0\right). \tag{2.70}$$

In a ferromagnetic material, the elastic deformation disturbs the steady magnetization state, because it varies a particular magnetic domain volume or affects the electron's subshell orbits, resulting in an additional flux magnetic density. This is the reversed magnetostriction mechanism (piezomagnetic effect). The constitutive relation will take the form

$$B_i = \mu_0 \mu_{ij}^S H_j + \tilde{e}_{iJ}^{(MS)} S_J, \quad (i,j = x,y,z;\ J = 1,2,\ldots,6) \tag{2.71}$$

Here, μ_{ij}^S is the normalized permeability tensor at a constant strain. The piezomagnetic coefficients $\tilde{e}_{iJ}^{(MS)}$ relate the induced magnetic flux density to the applied strain field. Equation (2.71) is similar to the constitutive equation for expressing the piezoelectric effect (Auld 1973). We know from the thermodynamics of solids that the piezoelectric strain matrix is a transposed matrix of the converse piezoelectric stress matrix. An analogous relationship is expected for the piezomagnetic coefficients:

$$\tilde{e}_{iJ}^{(MS)} = e_{Ji}^{(MS)}. \tag{2.72}$$

Experiments indicate that Eq. (2.72) holds roughly, but not exactly.

Returning to the two-dimensional approximation, we obtain a differential equation for E_y by substituting Eq. (2.70) into Eq. (2.1) and eliminating H_x and H_z using Eqs. (2.2) and (2.71). It gives a general solution of the electric field in the material. (Also, it applies to obtain the electric field in a vacuum using zero conductivity and zero elastic displacement.) The general solutions include arbitrary constants. The boundary conditions at the moving surface are (Il'in and Kharitonov 1981)

$$\mathbf{n}_0 \times (\mathbf{E}^V - \mathbf{E}) = \frac{\partial u_3}{\partial t} (\mathbf{B}_0^V - \mathbf{B}_0), \tag{2.73}$$

$$\mathbf{n}_0 \times (\mathbf{H} - \mathbf{H}^V) = \mathbf{n}' \times (\mathbf{H}_0^V - \mathbf{H}_0). \tag{2.74}$$

These allow us to determine the constants and obtain the electric field in vacuum, which can be detected by an EMAT coil. Here, $\mathbf{n}_0$ is an outward unit vector normal to the surface and $\mathbf{n}'$ is the one when the surface is perturbed by the ultrasonic wave. The detailed calculation procedure was given by Ogi (1997).

2.4 Comparison with Measurements

The Lorentz forces are proportional to the applied magnetic field. The magnetization forces are proportional to the magnetization magnitude. Both of them increase monotonically with the applied field. The magnetostriction forces, however, are complicated functions of the field depending on material's magnetostriction

response to the field. The above theoretical model can be confirmed by measuring the magnetic field dependence of ultrasonic wave amplitude, because the body forces produce acoustic waves through Eq. (2.5) and are proportional to the generated waves.

2.4.1 SH Plate Wave

Figure 2.6 shows an EMAT configuration to generate a shear-horizontal (SH) plate wave via the magnetostriction mechanism. It consists of a meander-line coil and a static magnetic field along the straight parts of the coil. Neither a Lorentz force nor a magnetization force occurs with this configuration. This type of EMAT was reported first by Thompson (1979). Considering the two-dimensional model in Fig. 2.1b and the stress-free condition $\sigma_4 = 0$ at the surface, it is easy to find that only the magnetostriction force

$$f_y^{(MS)} = \frac{\partial \sigma_6^{(MS)}}{\partial x} = -e_{6x}^{(MS)} \frac{\partial H_x}{\partial x}, \tag{2.75}$$

contributes to the SH wave generation. The field dependence of the wave amplitude is governed by that of the coefficient $e_{6x}^{(MS)} = c_{66} d_{6x}^{(MS)}$. $d_{6x}^{(MS)}$ is given by Eq. (2.66) and c_{66}, a shear modulus, is known; and the coefficient can be calculated as a function of the field using the measurable magnetostriction curve (ε_t-H_0 curve).

For an interstitial-free steel, the field dependence of the SH wave amplitude was measured. As shown in Fig. 2.6, the SH wave was launched by the EMAT and

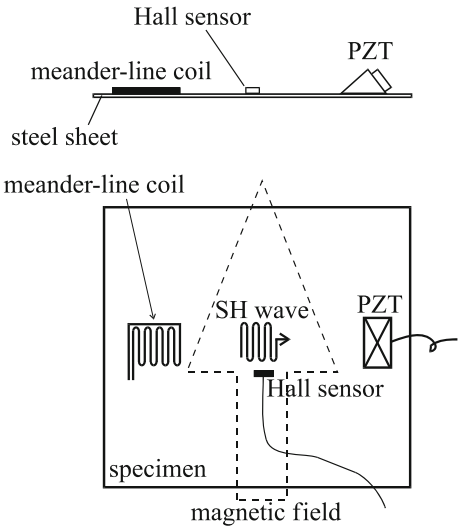

Fig. 2.6 Generation of SH plate wave with a meander-line-coil EMAT and detection of it with a PZT transducer. The tangential biasing field was applied using an electromagnet

detected by a wedge-mounted piezoelectric transducer. A Hall sensor detected the static field. The magnetostriction along the field was measured by a semiconductor strain gauge. We found that the magnetostriction curve can be well approximated by the following function as shown by the solid line in Fig. 2.7a

$$\varepsilon_t = 34H^{0.2} \times 1.48^{-1.5(H+1)} - 5.5, \tag{2.76}$$

where ε_t is in microstrain and H in 10^4 A/m.

Figure 2.7b compares the measurements with the calculated coefficient. They are principally consistent, showing the peak near the maximum magnetostriction, a minimum at the zero magnetostriction at the field of $\sim 2.4 \times 10^4$ A/m, and a gradual increase to high fields. Thus, the theory essentially explains the measurements. There are, however, discrepancies in magnitude between the theory and measurements; the measurements are lower than the calculations in low fields and larger in high fields. This may be attributed to the electromagnetic losses, including the hysteresis loss due to irreversible movement of magnetic domains and the eddy current loss (or the Joule-heating loss). They occur when the ferromagnetic material is dynamically magnetized and are closely related to the susceptibility of the material (Chikazumi 1964): high susceptibility causes high losses. Susceptibility is higher and the losses are more remarkable in the low-field region than in the high-field region.

When the bias magnetic field is applied in an angled direction by ϕ about the straight parts of the meander-line coil (in the y-axis) as shown in Fig. 2.8, similar expressions for the piezomagnetic coefficients to Eqs. (2.65) and (2.66) are

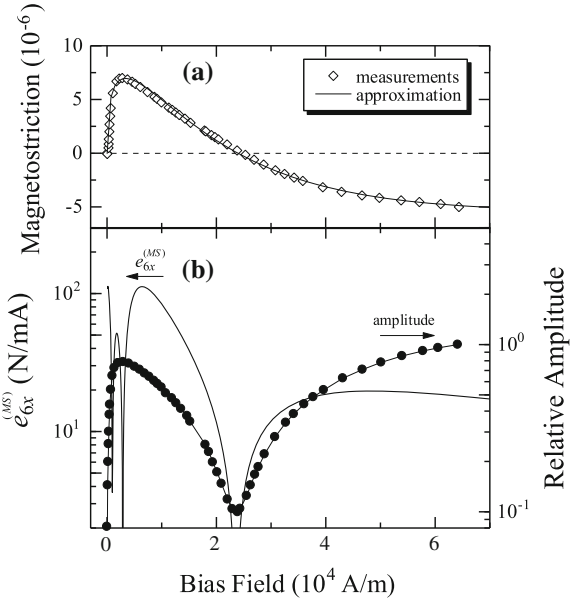

Fig. 2.7 **a** Magnetostriction curve of an interstitial-free steel. *Open marks* denote measurements and the *solid line* is an approximation given by Eq. (2.76). **b** Comparison between the field dependence of the SH plate wave amplitude generated by the EMAT and the calculated piezomagnetic coefficient, $e_{6x}^{(MS)}$

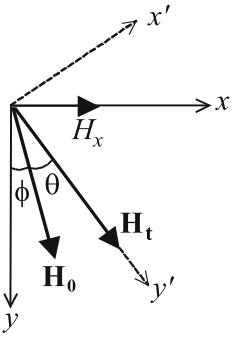

Fig. 2.8 Oblique bias magnetic field in the *y*-axis

obtained by replacing θ with θ + ϕ, H_{0y} with $H_{0y}\cos\phi$, and H_x with $H_x + H_0\sin\phi$. For example,

$$d_{6x}^{(MS)} = \frac{3\gamma}{2}\sin 2(\theta+\phi)\sin(\theta+\phi) + \frac{3\varepsilon_t}{H_{0y}\cos\ \phi}\cos^2(\theta+\phi)\cos\ 2(\theta+\phi). \quad (2.77)$$

The resulting SH wave amplitude is proportional to $e_{6x}^{(MS)}$ and its dependence on the inclined angle of the bias magnetic field, ϕ, can be calculated. Figure 2.9a presents such calculations of coefficient $e_{6x}^{(MS)}$, showing a maximum in the range of ϕ = 45°–60°, which depends on the relative magnitude between ε_t and γ. The corresponding measurements are shown in Fig. 2.9b, which supports the calculation. Thus, an

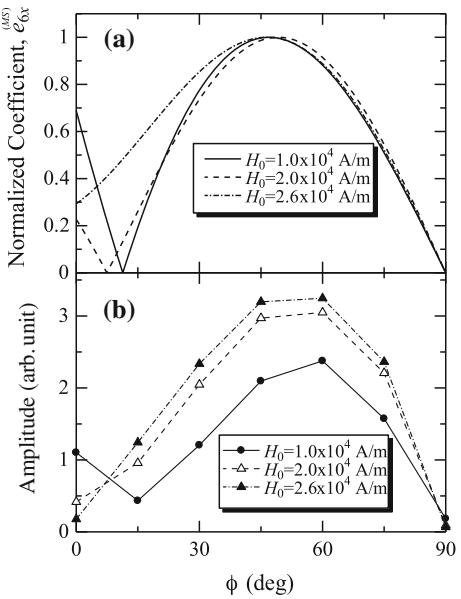

Fig. 2.9 Dependence of **a** the piezomagnetic coefficient $e_{6x}^{(MS)}$ and **b** the SH wave amplitude on the direction of the bias magnetic field. (After Ogi et al. 2003)

oblique static magnetic field is quite effective to increase the efficiency of this type of EMAT as shown in Fig. 3.13.

2.4.2 Bulk Shear Wave

A bulk shear wave can be excited when the tangential field is applied normal to the straight parts of the meander-line coil (i.e., in the x direction in Fig. 2.1b). It propagates perpendicular to the specimen surface with a polarization parallel to the surface. The electromagnetic ultrasonic resonance (EMAR) technique described in Chap. 5 was used to measure the normalized amplitude of the bulk shear wave as a function of the tangential field for a low-carbon steel. The result is shown in Fig. 2.10.

The Lorentz force mechanism will not contribute to the shear wave generation. (It can generate the longitudinal wave, however.) The magnetostriction force that contributes to the bulk shear wave generation is

$$f_x^{(MS)} = \frac{\partial \sigma_5^{(MS)}}{\partial z} = -e_{5z}^{(MS)} \frac{\partial H_z}{\partial z}. \tag{2.78}$$

Thus, the normal component of the dynamic field, H_z, which occurs between the straight parts of the coil, plays an important role for the generation as illustrated in Fig. 2.11. The coefficient $e_{5z}^{(MS)}$ equals $C_{55} d_{5z}^{(MS)}$ and the form of $d_{5z}^{(MS)}$ is essentially the same as that of $d_{6x}^{(MS)}$ in Eq. (2.66), where H_{0y} has to be replaced by H_{0x}. Figure 2.10 shows the calculation of the coefficient using the material's magnetostriction response. Again, the measurements and calculation are compared favorably with each other.

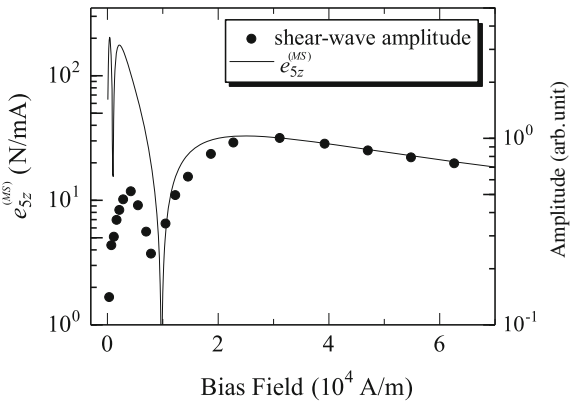

Fig. 2.10 Field dependence of the shear wave amplitude and that of the piezomagnetic coefficient, $e_{5z}^{(MS)}$

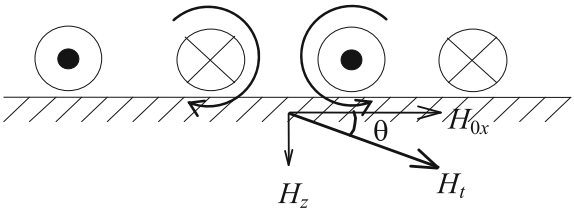

Fig. 2.11 Inclined total magnetic field about the static field direction by θ to cause shear wave traveling in the z direction

References

Auld, A. B. (1973). *Acoustic Fields and Waves in Solids*. New York: Wiley.

Beissner, R. E. (1976). Electromagnetic-acoustic transducers: A study of the state-of-the-art. *Southwest Research Institute*, Report NTIAC-76–1.

Brown, W. F., Jr. (1966). *Magnetoelastic Interactions* (p. 57). Berlin: Springer.

Chikazumi, S. (1964). *Physics of Magnetism*. New York: Wiley-Interscience.

Gaerttner, M. R., Wallace, W. D., & Maxfield, B. W. (1969). Experiments relating to the theory of magnetic direct generation of ultrasound in metals. *Physical Review, 184*, 702–704.

Hammond, P., & Sykluski, J. K. (1994). *Engineering Electromagnetism Physical Processes and Computation* (pp. 155–165). Oxford: Oxford Science Publications.

Il'in, I. V., & Kharitonov, A. V. (1981). Theory of the EMA method of detecting Rayleigh waves for ferromagnetic and ferrimagnetic materials. *Soviet Journal of Nondestructive Testing-USSR, 16*, 549–554.

Kawashima, K. (1976). Experiments with two types of electromagnetic ultrasonic transducers. *The Journal of the Acoustical of America, 60*, 365–373.

Kawashima, K. (1985). Electromagnetic acoustic wave source and measurement and calculation of vertical and horizontal displacements of surface waves. *IEEE Transaction on Sonics and Ultrasonics, SU-32*, 514–522.

Maxfield, B. W., & Fortunko, C. M. (1983). The design and use of electromagnetic acoustic wave transducers (EMATs). *Materials Evaluation, 41*, 1399–1408.

Moon, F. C. (1984). *Magneto-Solid Mechanics*. New York: Wiley-Interscience.

Ogi, H. (1997). Field dependence of coupling efficiency between electromagnetic field and ultrasonic bulk waves. *Journal of Applied Physics, 82*, 3940–3949.

Ogi, H., Goda, E., & Hirao, M. (2003). Increase of efficiency of magnetostriction SH-wave EMAT by angled bias field: Piezomagnetic theory and measurement. *Japanese Journal of Applied Physics, 42*, 3020–3024.

Ogi, H. (2012). Erratum: "Field dependence of coupling efficiency between electromagnetic field and ultrasonic bulk waves" [*J. Appl. Phys*. **82**, 3940 (1997)]. *Journal of Applied Physics, 112*, 059901.

Ribichini, R., Nagy, P. B., & Ogi, H. (2012). The impact of magnetostriction on the transduction of normal bias field EMATs. *NDT & E International, 51*, 8–15.

Seher, M., & Nagy, P. B. (2016). On the separation of Lorentz and magnetization forces in the transduction mechanism of Electromagnetic Acoustic Transducers (EMATs). *NDT & E International*, *84*, 1–10.

Thompson, R. B. (1973). A model for the electromagnetic generation and detection of Rayleigh and Lamb waves. *IEEE Transaction on Sonics and Ultrasonics*, *SU-20*, 340–346.

Thompson, R. B. (1977). Mechanism of electromagnetic acoustic generation and detection of ultrasonic Lamb waves in iron-nickel alloy polycrystals. *Journal of Applied Physics, 48*, 4942–4950.

Thompson, R. B. (1978). A model for the electromagnetic generation of ultrasonic guided waves in ferromagnetic metal polycrystals. *IEEE Transaction on Sonics and Ultrasonics, SU-25*, 7–15.

Thompson, R. B. (1979). Generation of horizontally polarized shear-waves in ferromagnetic materials using magnetostrictively coupled meander-coil electromagnetic transducers. *Applied Physics Letters, 34*, 175–177.

Thompson, R. B. (1990). Physical principles of measurements with EMAT transducers. In *Physical Acoustics* (Vol. 19, pp. 157–200). New York: Academic Press.

Wilbrand, A. (1983). EMUS-probes for bulk waves and Rayleigh waves. Model for sound field and efficiency calculations. In *New Procedures in Nondestructive Testing* (pp. 71–80). Berlin: Springer.

Wilbrand, A. (1987). Quantitative modeling and experimental analysis of the physical properties of electromagnetic-ultrasonic transducers. In *Review of Progress in Quantitative Nondestructive Evaluation* (Vol. 7, pp. 671–680).

http://www.springer.com/978-4-431-56034-0

Electromagnetic Acoustic Transducers
Noncontacting Ultrasonic Measurements using EMATs
Hirao, M.; Ogi, H.
2017, XVI, 380 p. 287 illus., 44 illus. in color., Hardcover
ISBN: 978-4-431-56034-0